sustainability

MDPI

Article

Green Synthesis and Characterization of Zinc Oxide Nanoparticles Using *Larrea tridentata* Extract and Their Impact on the In-Vitro Germination and Seedling Growth of *Capsicum annuum*

Daniela Monserrat Sánchez-Pérez [1], Erika Flores-Loyola [2], Selenne Yuridia Márquez-Guerrero [1], Magdalena Galindo-Guzman [3] and Jolanta E. Marszalek [2,*]

[1] Programa Agua-Suelo, National Technological Institute of Mexico, Technological Institute of Torreón (ITT)-DEPI, Graduate Studies and Research Division, Torreón 27190, Mexico
[2] Faculty of Biological Sciences, Autonomous University of Coahuila, Torreón 27276, Mexico
[3] Polytechnic University of the Laguna Region, San Pedro de las Colonias 27942, Mexico
* Correspondence: j.marszalek@uadec.edu.mx

Abstract: The application of green methods in the synthesis of nanoparticles using plants is a cost-effective and eco-friendly approach. Zinc oxide nanoparticles are of great importance due to their versatile properties. The conditions of synthesis strongly influence the characteristics and functionality of the nanoparticles. The present work studied the biological, green synthesis of zinc oxide nanoparticles (ZnONPs) in the presence of different concentrations of ethanolic extract of *Larrea tridentata* (10, 20, and 30 mg/mL). The time of the formation of nanoparticles was evaluated at different temperatures and pH values of the reaction medium. The formation of ZnONPs was confirmed by ultraviolet-visible (UV-Vis) and Fourier transform infrared spectroscopies (FT-IR), as well as scanning electron microscopy (SEM). X-ray diffraction analysis (XDR) determined the crystallographic structure of the nanoparticles. Obtained ZnONPs had a size range of 18 to 40 nm. The temperature, reaction time, and pH significantly influenced the nanoparticles' morphology, size, and aggregation. The impact of chosen ZnONPs was tested on the germination of serrano chili seeds (*Capsicum annuum*). At 100 ppm, the nanoparticles improved germination percentage, vigor, and seedlings' growth parameters.

Keywords: ZnO nanoparticles; green synthesis; *Larea tridentata*; germination

Citation: Sánchez-Pérez, D.M.; Flores-Loyola, E.; Márquez-Guerrero, S.Y.; Galindo-Guzman, M.; Marszalek, J.E. Green Synthesis and Characterization of Zinc Oxide Nanoparticles Using *Larrea tridentata* Extract and Their Impact on the In-Vitro Germination and Seedling Growth of *Capsicum annuum*. *Sustainability* **2023**, *15*, 3080. https://doi.org/10.3390/su15043080

Academic Editor: Farid Menaa

Received: 16 December 2022
Revised: 24 January 2023
Accepted: 1 February 2023
Published: 8 February 2023

1. Introduction

Green nanoparticle synthesis technology is an attractive method for the formation of nanomaterials because of its eco-friendly, low-cost, low-energy, and often single-step approach. Nanotechnology is a developing science that has gained significant importance due to its multiple applications in a variety of areas, including textile industries [1], cosmetics [2], food, and agriculture [3], among others. Zinc oxide nanoparticles (ZnONPs), whose sizes range from 1 to 100 nm, have been widely studied as strategic, functional inorganic materials [4]; antimicrobial agents [5]; and as catalytic [6], electric, optoelectric [7], and photochemical stimuli [8]. These NPs also act as a regulatory cofactor in plant-protein and tryptophan synthesis [9]. In recent years, the agroindustry has implemented the use of ZnONPs as plant stimulants and micro-fertilizers [5]. Plants can more easily absorb chemical compounds presented in the form of NPs because of their size and the ease with which they penetrate the tissues compared to the bulk forms [10]. When NPs are applied to plants, various effects can occur, such as inducement or inhibition of seeds' germination and seedling growth [11], activation of genes involved in metabolism [12], stimulation of photosynthesis [13], reactive oxygen species generation, and chromosomal aberrations [14]. Specifically, zinc is an essential nutrient for plant growth which plays a

critical role in metabolisms in stimulating enzymes such as carbonic anhydrase, aldolase, and hydrogenase [15]. Principally, during early growth stages, a zinc deficit could retard seedling growth. In addition, it affects the capacity for water uptake; soaking seeds in zinc solutions could improve moisture retention, favoring germination. Furthermore, zinc is involved in the production of tryptophan and auxin, essential growth hormones, which could enhance plants' yield and quality [15–17].

However, the above benefits generally depend on the size, size distribution, and morphology of the ZnONPs, which are related to factors involved in their synthesis, such as the concentration of precursor reagents, pH, and temperature, among others [18]. Different physical and chemical processes can be used to synthesize these nanoparticles. The most common is chemical synthesis, which uses metal precursors, reducing agents, and often stabilizing molecules, to form stable and well-defined nanoparticles [19]. In this process, the reducing agents can be sodium citrate, ascorbate, sodium borohydride ($NaBH_4$), elemental hydrogen, or poly(ethylene glycol) block copolymers [8]. However, those chemicals produce toxic residues [20] which are unfriendly to the environment, demand high energy, and are usually expensive [21].

On the other hand, the green synthesis of nanoparticles aims to reduce and eliminate polluting residues and introduces materials and processes that are better for the environment, more efficient, more feasible, and require less applied energy [22,23]. The NPs can be synthesized in the presence of plant extracts (for example, banana leaves, garlic plants, aloe, basil, and medical plants) that naturally possess bioactive components capable of reducing and stabilizing the arising nanoparticles [24–28]. Qualitative studies of biochemical compounds indicate that various metabolites such as terpenoids, phenolic compounds, flavonoids, aldehydes, ketones, enzymes, proteins, and carbohydrates participate as reducing agents in the synthesis of metallic NPs, as they are able to donate electrons and reduce the metallic ions into elemental metals in nanoparticles [29,30]. These biocompounds contain several functional groups, such as hydroxyl, carboxyl, and amine, which react with metal ions to reduce them into metallic atoms. In addition, these compounds assist in the coating of formed nanoparticles, giving them stability in the solution, biocompatibility, and possibly additional functionality in applications [31].

Creosote bush (*Larrea tridentata*), also known as greasewood and chaparral in the USA and gobernadora in Mexico, is a bush growing in semidesert regions of the southwestern United States and northern Mexico. High concentrations of those abovementioned bioactive antioxidant compounds have been shown in its extracts [25,32,33], among which lignans are the most dominant. Nordihydroguaiaretic acid (NDGA) is an extensively studied lignan with antibacterial, antiviral, anthelmintic, antifungal, and anticancer properties [34,35]. Furthermore, the biocomponents from *L. tridentata* extracts stabilize the NPs during the synthesis as they modify their surface [36]. As of now, aqueous *L. tridentata* extracts have been used in silver [25,37] and Cu/CuO [38] nanoparticle syntheses. Unfortunately, aqueous extraction limits the successful removal of some crucial biocompounds from the plant, as they have limited solubility in water [39]. In addition, in the literature, none of the synthesis parameters were evaluated to improve nanoparticle quality. For this reason, a green methodology to synthesize ZnONPs using an ethanolic extract of *L. tridentata* is studied in the present work, evaluating different extract concentrations, as well as the influence of temperature, and pH, on nanoparticle formation. As an example of ZnONPs application, we present their influence on the germination of serrano chili seeds (*Capsicum annuum*).

2. Materials and Methods

For the NPs synthesis, hexahydrate zinc nitrate (Sigma-Aldrich, Saint Louis, MI, USA) as precursor salt, reagent grade sodium hydroxide (Fagalab, Favela Pro, S.A. de C.V., Mocorito, Mexico), and 96% ethyl alcohol (CTR scientific, Monterrey, Mexico) were used as received. For LTE (*Larrea tridentata* extract) preparation, fresh plants collected from ejido Rancho Alegre, in Torreon, Coahuila, Mexico in the summer of 2021 (25°29′31 N 103°05′24 W) were used. Am-

berlite XAD16N cationic exchange resin (Sigma-Aldrich, Merck KGaA, Darmstadt, Germany) was used for the LTE purification.

2.1. Preparation of the Larrea Tridentata Extract (LTE)

The leaves of freshly cut *Larrea tridentata* were washed with purified water to remove impurities and dirt, then dried at 45 °C for 24 h, and subsequently crushed in a mortar. A total of 10 g of the crushed leaves were added to 100 mL of a 50% ethanolic solution and heated to 60 °C for 30 min; then, the solution was filtered. Finally, the crude extract was passed twice through a column packed with Amberlite XAD16N resin using 50% ethanolic solution as eluent.

Extract Characterization

The dry-matter concentration of LTE was obtained by placing 1 mL of the purified extract on a watch glass and drying it at 60 °C to constant weight. Infrared spectroscopy was used to identify the functional groups in the ethanolic extract of *Larrea tridentata*. For this, the sample was prepared by placing an aliquot of 100 µL in 100 mg of KBr powder and drying it in an oven for 24 h at 40 °C. The KBr/extract pellet was prepared and analyzed using an FTIR spectrometer (FTIR NICOLET FTIR-100,Thermo Fisher Scientific, Monterrey, Mexico) in a region from 4000 to 400 cm^{-1} with a resolution of 4 cm^{-1}. The optical properties of LTE were determined by UV-Vis spectroscopy, for which the extract was diluted in water in a 1:10 ratio, using distilled water as a blank. In addition, LTE at different pH values was prepared by adjusting the pH with concentrated HCl or NaOH solutions, keeping the amount of the extract constant. The total phenols content was estimated by the colorimetric method of Folin-Ciocalteu and expressed as gallic acid equivalents on a fresh-weight basis (GAE/g fw) [40]. The antioxidant capacity of the extract was determined by the DPPH (2,2-diphenyl-1-picryl-hydrazyl-hydrate) assay according to the methodology described by Brand-Williams and expressed as mg of Trolox g^{-1} fw [41]. Analyses were performed in triplicate.

2.2. Green Synthesis of Zinc Oxide Nanoparticles

For the green synthesis of zinc oxide nanoparticles, the methodology reported by Selim et al. [42] with some modifications was followed. Three extract concentrations (10, 20, and 30 mg/mL) and three temperatures (55, 70, and 85 °C) were used in ZnONPs synthesis. The pH was adjusted to 4.5, 7, and 13 by adding NaOH/HCl solutions. In a typical synthesis, 20 mL of purified LTE was added to 200 mL of 1.5 mM zinc nitrate solution at the desired temperature. The synthesis process was followed with UV-Vis spectroscopy. For that, 1 mL aliquot was taken every 2 h during the 24 h reactions and every 15 min during the 2 h reactions. The spectra were recorded in the range of 200 to 700 nm.

At the end of the reaction, the resulting mixture presented a white precipitate containing the ZnONPs. They were recovered by centrifugation at 4500 rpm for 15 min and then washed with 50% aqueous ethanol solution and, subsequently, with distilled water. These NPs were resuspended in distilled water for subsequent analysis. To evaluate the yield of the reaction, a nanoparticle-solution aliquot was dried at 60 °C for 24 h and weighed.

ZnONP Characterization

The NPs synthesized in the presence of LTE were characterized by UV-visible and FTIR spectroscopies, X-ray diffraction, DLS, and scanning electron microscopy. The optical properties of the purified nanoparticles were examined using a UV-visible spectrometer (JENWAY MODEL 7305, TEquipment, Long Branch, NJ, USA) in the spectral range of 200–700 nm and 2 nm resolution. The functional groups present in the synthesized nanoparticles were determined using an FTIR spectrometer (FTIR NICOLET FTIR-100, Thermo Fisher Scientific, Monterrey, NL, Mexico) in a region of 4000 to 400 cm^{-1} using the KBr pellet method with a resolution of 4 cm^{-1}. X-ray diffraction analysis (XRD) was carried out in an X-ray diffractometer PANalytical, Malvern Panalytical, Madrid, Spain,

Empyrean with copper radiation Kα with wavelength, λ = 1.5406 Å. The goniometer was operated from 5° to 90° in 2θ and the scan speed was 30 s with a step of 0.026°. The phases present were identified using ICSD (Inorganic Crystal Structure DataBase) diffraction charts and HighScore Plus software https://www.fiz-karlsruhe.de/en/produkte-und-dienstleistungen/inorganic-crystal-structure-database-icsd (accessed on 3 March 2022). The morphology and size of the NPs were determined with a scanning electron microscope TESCAN MIRA (TESCAN ORSAY HOLDING, a.s., Brno, Czech Republic) with field emission filament (FEG) under vacuum conditions. The acquired images were analyzed using the GIMP 2.0 software https://www.gimp.org/ (accessed on 7 September 2022). Dynamic light scattering analysis (DLS) was used to determine the average size, polydispersity (PDI), and zeta potential of the ZnONPs. The liquid samples were diluted in DI water, sonicated for 4 h, and transferred to a cell. The analysis was performed with Laser Diffraction Particle Size Analyzer LA-960–HORIBA (HORIBA Scientific, Kyoto, Japan) at room temperature.

2.3. Seed Germination Testing

The tests were conducted using serrano chili seeds (*Capsicum annuum*) purchased from Rancho Los Molinos S.A de C.V. (Cuernavaca-Tepoztlan, Morelos, Mexico). The seeds were washed with 70% ethanol for 2 min, then washed 3 times with distilled water [11]. Germination tests were performed by placing 10 seeds per 8 cm diameter Petri dish containing a filter paper. The seeds were impregnated with 5 mL of each treatment. The six applied treatments were 0, 50, 100, 150, 200, and 250 ppm ZnONPs (synthesized at 70 °C and pH of 13, from 30 mg/mL extract in 4 h). Each test was performed in triplicates. The Petri dishes were sealed with Parafilm paper and placed in a Novatech CA-550 artificial growth chamber (NOVATECH, San Pedro, Tlaquepaque, Mexico) at 26 °C with a 12 h day/night cycle for 7 days [43].

Physiological Indexes of Seedlings

The following measurements were taken after 7 days: seed vigor index, the percentage of germination (%), the length of the root (mm), fresh weight of plumule (epicotyl), and root (mg) [43]. The fresh weight of the plumule and root was weighed on an analytical scale and reported in milligrams per plumule. Seedling vigor was calculated as a germination percentage by seedlings' length in cm (root + shoot) [7,44]. The germination percent (G%) was determined as the ratio of germinated seeds to the total number of seeds incubated [43,45]. Plumule length was measured from the radicle-hypocotyl intersection to the base of the cotyledon, while radicle length was measured from the base of the hypocotyl to the radicle apex.

2.4. Statistical Analysis

The experiment was conducted using a completely randomized design with six treatments and four repeats. The results obtained were analyzed using analysis of variance and comparison of means with Tukey's test ($p \leq 0.05$) using the statistical package Statistical Analysis System Institute (SAS) version 9.4 http://support.sas.com/software/94/index.html (accessed on 4 October 2022).

3. Results and Discussion

3.1. Extracts Characterization

The dry matter contained in the purified extract was 33 ± 0.12 mg/mL. At this dry-mass concentration, the total phenol content was 2473.24 ± 1.37 mg GAE g^{-1} fw, and the antioxidant capacity was 565.61 ± 0.41 mg of Trolox g^{-1} fw (Table 1). Salayova et al. [24] found lower total phenols content in the aqueous extract of *L. tridentata*. However, it has been shown that some of the bioactive compounds of *L. tridentata* are more soluble in organic solvents [32]. Solvents such as ethanol result in higher biomolecule extraction and, thus, higher total phenol content and antioxidant capacity. *L. tridentata* extracts have been successfully used for nanoparticle synthesis [25], showing their potential to reduce zinc

ions into zinc oxide nanoparticles. Surprisingly, when the extract was diluted to the 20 and 10 mg/mL concentrations, their characteristics did not follow the same decrease in their values. The concentration of the extracts was lowered by 33% and 66%, but the antioxidant activity only dropped by 4% and 10% for 20 mg/mL and 10 mg/mL, respectively. This indicates that the compounds in the LTE have potent antioxidant properties which are not necessarily related to their concentration. In *L. tridentata*, the antioxidant biomolecules are manifested by lignans, flavonoids, condensed tannins, and other polyphenolics [46–48]. The main lignan of LTE is nordihydroguaiaretic acid [1,4-bis (3,4-dihydroxyphenyl)-2,3-dimethyl-butane] (NDGA). Its structure is a polyphenol system with four phenolic hydroxyl groups, which supports radical scavenging [35,49].

Table 1. Content of total phenolic compounds of *Larrea Tridentata* extract and antioxidant capacity for different concentrations of dry matter.

Extract Concentration mg ml^{-1}	DPPH mg of Trolox g^{-1} fw	Total Phenols mg GAE g^{-1} fw
10	510.14 ± 0.71 c	1724.27 ± 2.75 c
20	535.61 ± 0.84 b	2215.44 ± 2.55 b
30	565.61 ± 0.41 a	2473.24 ± 1.37 a

Values are shown as mean values of three replicates with standard deviation. Values with different letters indicate a significant difference according to Tukey's test ($p \leq 0.05$).

Figure 1 shows UV-Vis spectra of LTE at different pH values. The structural and chemical change that occurs under different acidic conditions is observed in the peaks' shifts in the 250–400 nm range. The absorption in this region is typically attributed to compounds with conjugated π-bond systems and heteroatoms with non-bonding electron pairs [50,51], as found in polyphenols. In the spectra of the extract at pH values of 4.5 and 7, a peak at 345–350 nm appears. This peak shifts to 390–400 nm in the extract at a pH of 13. We attribute this redshift to the deprotonation of the hydroxyl groups [52]. Hydroxyl groups are present in many of the bioactive compounds found in the LTE, as confirmed with FT-IR spectroscopy (Figure 2). These −OH groups are present in flavonoids, anthocyanins, terpenoids, and, most importantly, lignans. NDGA is the primary representative of *L. tridentata* lignans because it is present in all parts of the plant, representing approximately 80% of all phenolics. NGDA has four hydroxyl groups at both ends of the molecule, which serve as a source of its antioxidant properties [35,53].

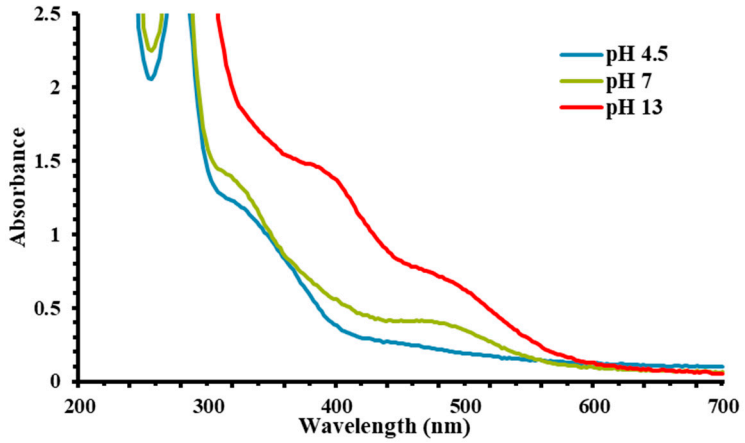

Figure 1. UV-visible spectra of *Larrea tridentata* extract at different pH values.

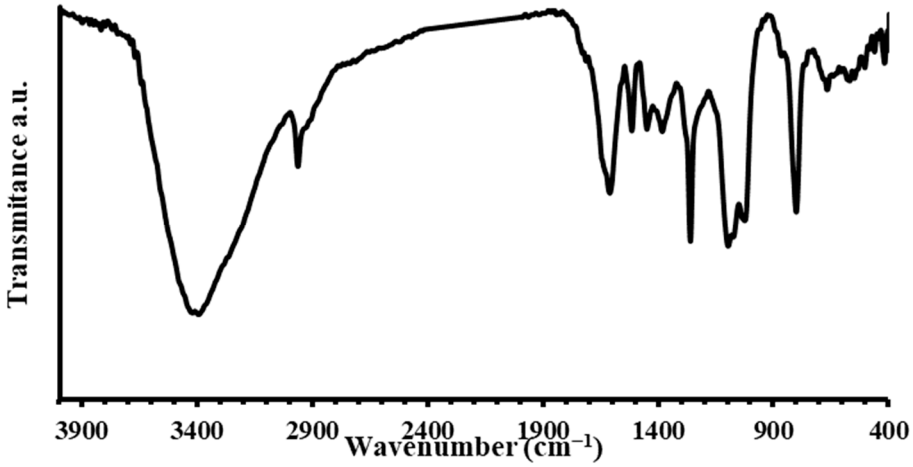

Figure 2. FT-IR spectra of the *Larrea tridentata* extract.

Bañuelos et al. [33] found that the main bioactive compounds in the ethanolic extract of *Larrea tridentata* are thymol and carvacrol. The FT-IR spectrum of the LTE prepared as a film on a KBr disc confirms the presence of groups of these two compounds (Figure 2). In the spectrum, a broad band between 3250 and 3500 cm^{-1} corresponds to the hydroxyl groups (−OH) present in carvacrol and thymol. The peaks in 2930–2830 cm^{-1} correspond to the symmetrical and asymmetrical vibrations of aliphatic $-CH_2-$ groups present in the phenolic compounds. In addition, a 1690 cm^{-1} band corresponds to the C=O stretching function attributed to ketones, carboxylic acids, and esters of other bioactive compounds. The 1200 cm^{-1} band corresponds to phenolic compounds, and 1050 cm^{-1} is a characteristic band of the C−O stretching of the phenols, such as thymol or carvacrol [33]. On the other hand, Cordova et al. [25] showed similar functional groups in the FTIR spectrum, varying only in intensity, from an aqueous extract of *Larrea tridentata*. The authors mentioned that the main bioactive compounds in their extract were anthocyanins, flavonoids, lignans, and terpenoids [25]. NDGA shows a set of characteristic bands: 740 cm^{-1} (C=C stretch, benzene ring stretching), 785 cm^{-1} (C=C rocking, benzene ring deformation), 1300 cm^{-1} (benzene ring breathing), 1607 cm^{-1} (in-plane C−O−H rocking), and 2900–3110 cm^{-1} (C-H stretching) [54]. The strong peak at 785 cm^{-1} confirms the presence of NDGA in our LTE.

3.2. Nanoparticles Synthesis and Characterization

During the reduction of zinc ions into zinc oxide nanoparticles, the yield of ZnONPs formation was evaluated. For each 1 g of zinc nitrate hexahydrate, 90 mg of zinc oxide nanoparticles are obtained with the use of the LTE at the 10 mg/mL concentration, 150 mg of ZnONPs for 20 mg/mL concentration, and 200 mg for 30 mg/mL concentration (synthesis conditions: 70 °C, pH = 13). These masses of ZnONPs represent the yield of ionic zinc conversion into zinc (in zinc oxide) within ZnONPs at 33%, 53%, and 73% for 10, 20, and 30 mg/mL extract concentrations, respectively. Thus, there is a direct correlation between the biocompounds' concentration in LTE and the amount of ZnONPs produced. With a higher concentration, there is a higher presence of antioxidants and biocompounds (phenols, flavonoids, and lignans) available for faster reduction, which would increase the conversion and concentration of ZnONPs in the system (Table 1) [55–57]. At the same time, we recognize that the antioxidant capacity of the LTE has limited influence on the syntheses' progression, since its values were on the same level for all of the extracts.

When the synthesis is followed with a UV-Vis spectrometer, as observed in Figure 3A, the increase in adsorption is three times faster for 30 and 20 mg/mL LTE concentrations than for the 10 mg/mL concentration reaction (based on the linear fit of the data of the initial 60 min). A similar trend can be seen in the first two hours of the NPs synthesis at a pH of 7 (Figure 3B), with the difference that the rate of NP formation at 20 mg/mL LTE concentration decreased by 80% with respect to the 30 mg/mL reaction. With the lowering

of the pH from 13 to 7, there might be a change in the access of some influential groups participating in the reduction of the zinc ions. In addition, in basic conditions, the −OH groups on polyphenols become alkoxides, as confirmed by UV-Vis, which can promote and support electron transfer. From the different conditions tested, it was determined that at a pH of 4.5, a minimal amount of zinc oxide NPs was formed. The lack of the synthesis of ZnONPs was corroborated by UV-visible spectroscopy (Figure 4), where the absorbance does not increase, as in the case of the other two syntheses, but rather rapidly decreases. In addition, the ZnONPs were very hard to recover during the centrifugation of the solutions at a pH of 4.5. The synthesis at higher pH agrees with the literature, which states that increasing the pH reduces the formation of agglomerates and the particle size [4,10,58].

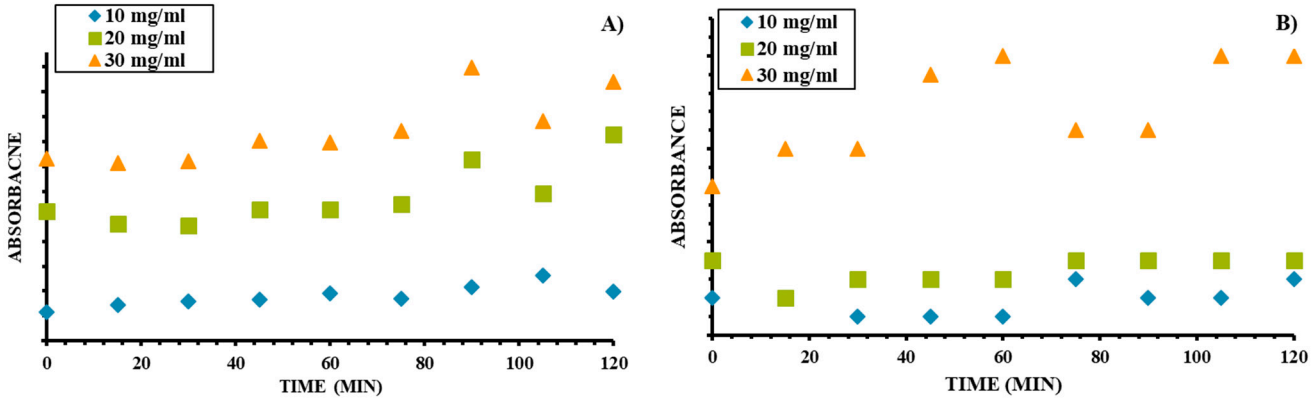

Figure 3. The change in absorbance (360 nm) with time during the synthesis of zinc oxide nanoparticles at 70 °C and (**A**) pH = 13 and (**B**) pH = 7.

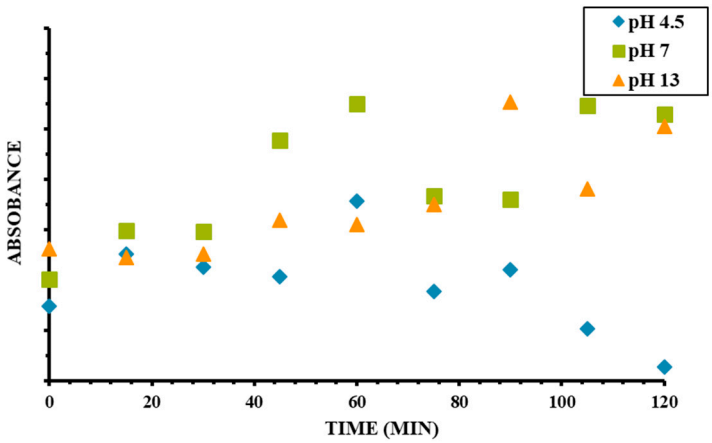

Figure 4. The change in absorbance with time during the synthesis of zinc nanoparticles using extract concentration of 30 mg/mL and temperature of 70 °C at different pH values of the medium.

The time of the ZnONPs synthesis has often been extended up to 24 h [59–63]. Therefore, we monitored the synthesis of ZnONPs for an extended time to determine the necessary reaction time that allows the formation of nanoparticles but prevents their significant agglomeration (Figure 5). The syntheses using 30 mg/mL extract and a pH of 13 at all temperatures (55°, 70°, and 85 °C) show an increase in absorbance in the first hours of the reaction and then a sharp decrease. We believe that the drop in absorbance is related to the beginning of the aggregation of the nanoparticles. The temperature is a significant kinetic factor for this reaction; thus, for synthesis at 55 °C, the initial formation occurs up to 16 h; at 70 °C, the nanoparticles without agglomeration form within 4 h; while at 85 °C, they form within the first 2 h. As the temperature increases, the nucleation rate that generates the NPs' formation increases; however, at the same time, it also favors the formation of agglomerates [18], as confirmed in the SEM images.

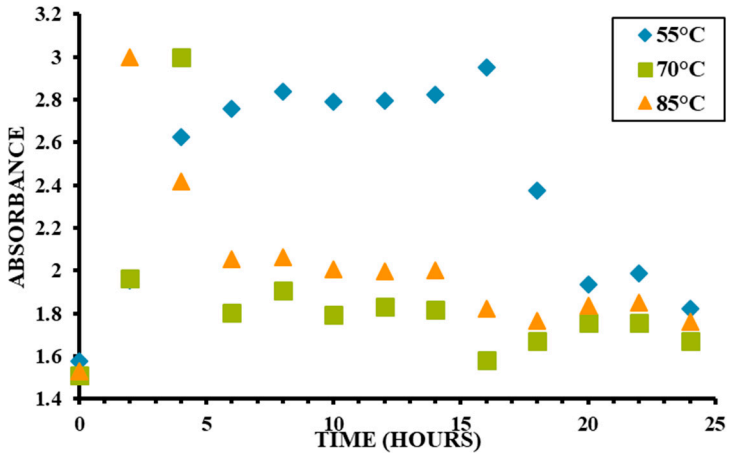

Figure 5. The change in the absorbance with time (24 h) at different temperatures; constant conditions: 30 mg/mL and pH = 13.

Another critical factor in ZnONPs synthesis is the reaction time. As presented in Figure 5, when agglomeration occurs, the adsorption of the system drastically drops; thus, with low temperatures, the formation of clusters can be avoided in synthesis for many hours. Moreover, when the reaction is carried out for prolonged times, after the adsorption drop, large-size agglomerated crystals are formed. For example, in reactions at 85 °C, the ZnONPs lump into giant crystals, as observed in the SEM images (Figure 6) [64]. As determined by this analysis, Singh et al. [57] reported that a fast synthesis resulted in smaller particles because short reaction times reduced the formation of the agglomerates. Thus, to save time and money and limit agglomeration, the synthesis of zinc oxide nanoparticles should be carried out at elevated temperatures, 70 °C or 85 °C, and time should be kept below 4 h.

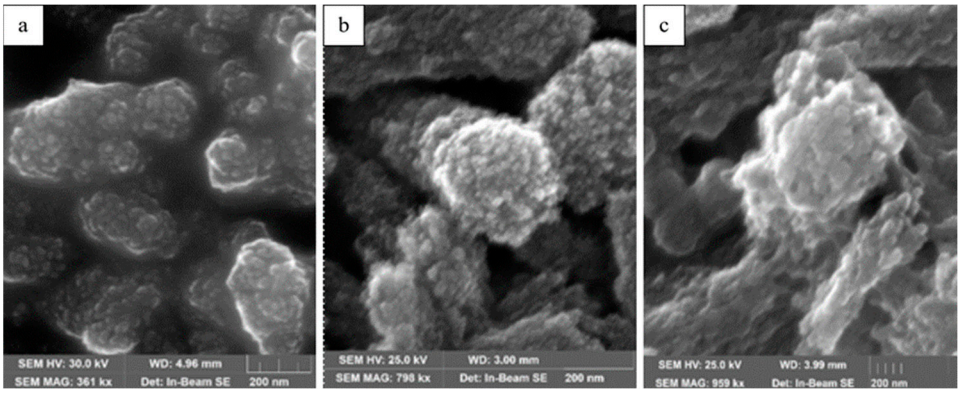

Figure 6. Scanning electron microscopy images of ZnONPs prepared at different temperatures. (**a**) 55 °C, 15 h; (**b**) 70 °C, 4 h; and (**c**) 85 °C, 2 h. Obtained at pH 13.

3.2.1. UV-Vis Spectroscopy

The UV-Vis spectra, in Figure 7, show a typical absorption peak for ZnONP at 358 nm for nanoparticles synthesized at pH 13 (30 mg/mL, 70 °C). The spectra of ZnONPs prepared at pH 4.5 and 7 do not show the same characteristic absorption band and have an absorption peak at 270 nm for pH 4 and 290 nm for pH 7. The literature reports an absorption peak for ZnONPs between 330–368 nm [65,66]. This characteristic absorption band is due to the excitation mode of their surface plasmon (SPR), which depends on the size of the nanoparticles. The nanoparticles' SPR bands experience a red or blue shift depending on their size [67,68]. On the other hand, Fakhari et al. [66] recognized that the position of the band gap increases with the reduction in particle size; therefore, the ZnONPs from 4.5 and 7 pH probably have very small sizes [4,66].

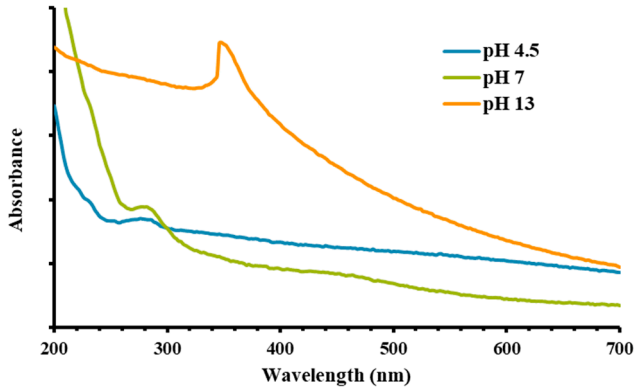

Figure 7. UV-Vis spectrum of purified ZnONPs, obtained at 70 °C for 4 h at different pH.

3.2.2. FTIR of the Nanoparticles

FT-IR spectroscopy (Figure 8) confirmed the presence of plant extract on the surface of zinc oxide NPs. The ZnONPs' spectra show bands at 461, 493, and 846 cm^{-1}, which are indicative of the stretching vibrations of the zinc and oxygen bonds, proving the presence of ZnO nanoparticles [69] since absorption peaks for the metal oxides are present in regions between 600 and 400 cm^{-1} [66]. The peak at 1500 cm^{-1} has been observed in ZnONPs, but at a higher wavenumber, 1616 cm^{-1}, and it has been assigned to O-H bending. Here, we believe it represents nanoparticles coating; a shoulder can be seen at a higher wavenumber indicating carbonyl stretching (1690 cm^{-1} in extract) on the surface of ZnONPs. Similarly, the broad absorption peak of 3440 cm^{-1} can be attributed to the characteristic absorption of hydroxyl, well represented in biocompounds of LTE. These data are similar to the results observed by others [45,70]. Furthermore, a band at 2925 and a peak at 1452 cm^{-1} come from the stretching and bending of C-H, respectively [67]. Thus, it is evident that the extract compounds, in addition to reducing zinc ions to ZnONPs, also work as a stabilizing agent and are present on the surface of the ZnONPs [25,45].

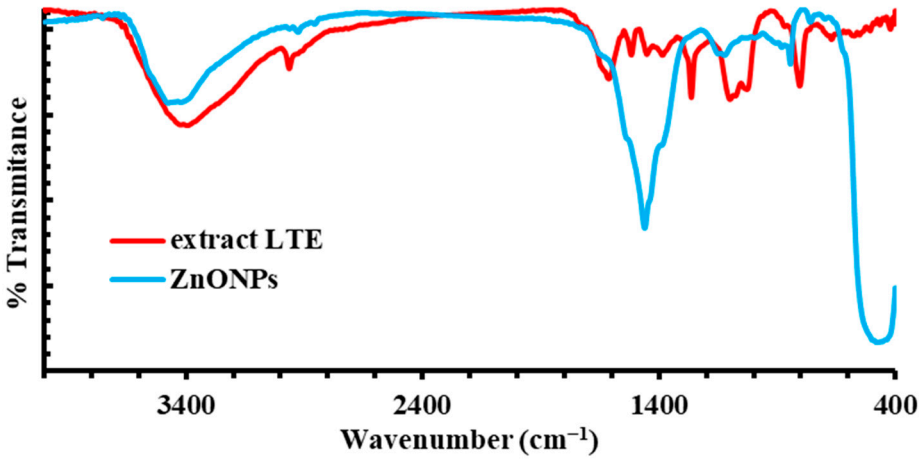

Figure 8. FTIR spectra, purified extract (– red line), and purified and dried ZnONPs (– blue line).

3.2.3. XDR

According to the diffractogram obtained by X-ray diffraction (XRD), no impurities are detected in the ZnONPs (Figure 9). The observed peak pattern represents the pattern of the zinc oxide (100, 002, 101, 102, 110, 103, 200, 112, and 201). The zinc oxide is in the zincite phase, which is hexagonal (ICSD, 98-005-7478). Therefore, the XRD pattern indicates that pure zinc oxide nanoparticles were obtained. Additionally, the diffraction peaks are narrow, indicating that the nanoparticles obtained are pure and crystalline.

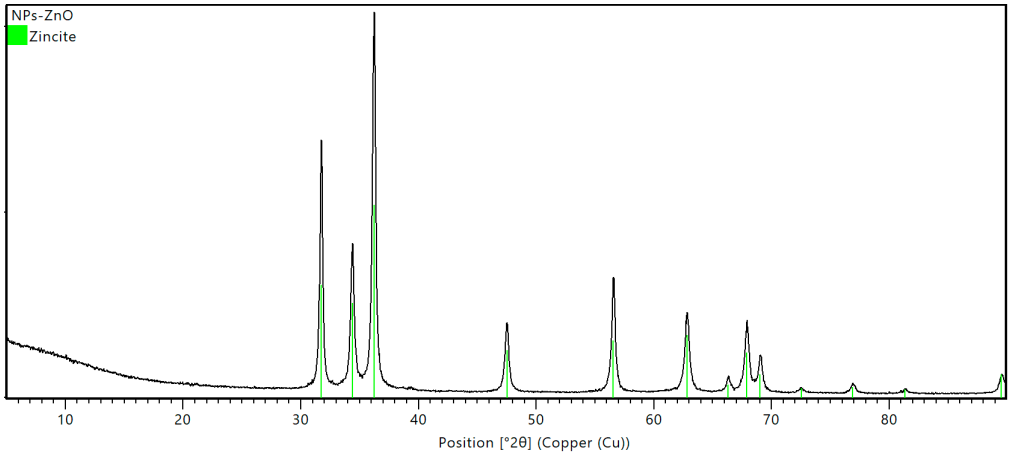

Figure 9. XRD analysis of ZnONPs obtained at 70 °C and pH = 13. The reference diffraction pattern of zinc oxide with hexagonal lattice (ICSD, 98-005-7478) is shown as green lines.

3.2.4. SEM

The SEM images showed that ZnONPs have a nanometric size, spherical shape, and uniform distribution. The images in Figure 10 show that using different concentrations of dry material in the extract does not influence the shape or size of ZnONPs (pH = 13 and 55 °C). Nanoparticles prepared at different extract concentrations have an average size of 28 ± 3.7 nm, and there is no statistical difference between them (Figures 10 and 11A). However, the nanoparticles prepared at different temperatures (pH = 13 and 30 mg/mL) vary in size (Figures 6 and 11B). ZnONPs synthesized at 85 °C are the largest, with an average size of 68 ± 4.3 nm, and their agglomerates consolidated (Figure 6C). As discussed above, this is due to the fact that an increased synthesis temperature accelerates the nucleation rate and, thus, the formation and growth of large crystals [18]. ZnONPs from the reaction at 70 °C are well-defined, with the smallest mean size of 18 ± 1.3 nm.

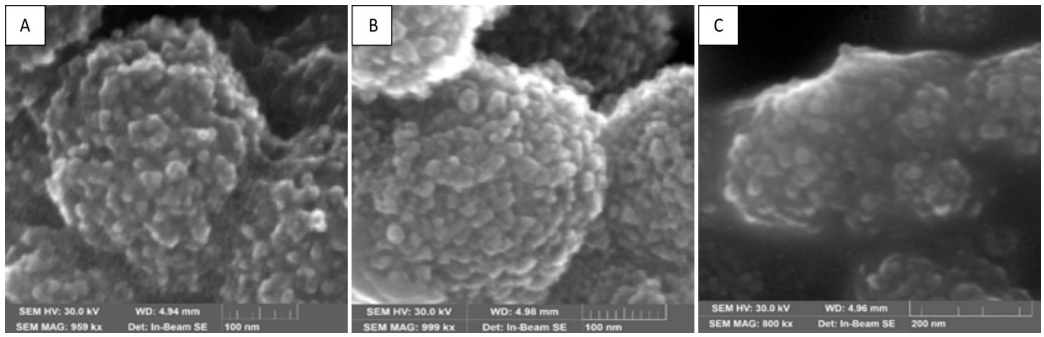

Figure 10. Scanning electron microscopy images of ZnONPs prepared with different concentrations of the extract. (**A**) 10 mg/mL, (**B**) 20 mg/mL, and (**C**) 30 mg/mL. Obtained at pH 13 and 55 °C.

On the other hand, nanoparticles synthesized at 55 °C possess a similar morphology to the previous ones, with an average particle size of 28 ± 4.8 nm (Figures 6A and 11). At the same time, the ZnONPs from the 55 °C reaction agglomerate to a higher degree than the others, possibly due to the reaction's extended time (15 h). Even though the NPs from the 70 and 85 °C reactions were collected before the aggregation of the nanoparticles should occur (as detected by the drop in absorbance in Figure 5), they still visibly accumulate into larger structures. Shariman et al. mentioned that longer reaction times lead to larger particles [64]. Consequently, we can conclude that high temperatures and short reaction times result in small ZnONPs [18].

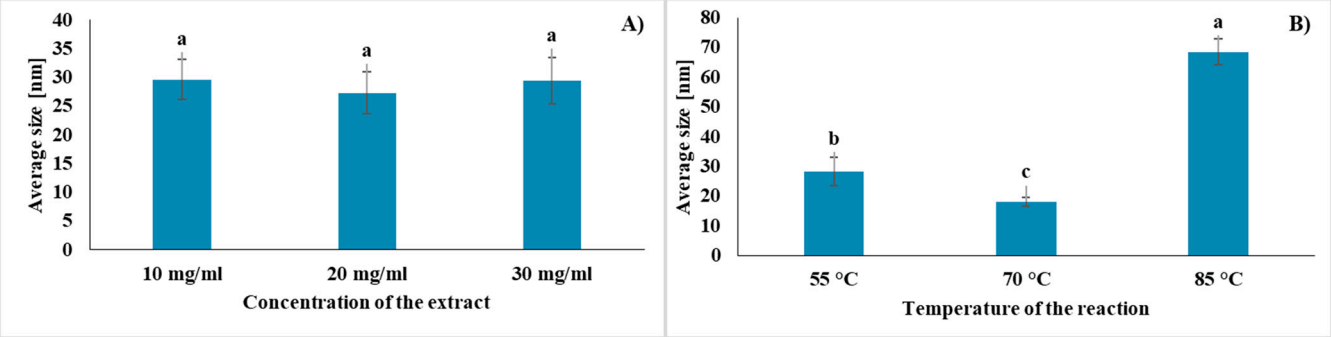

Figure 11. (**A**) An average size of the ZnONPs synthesized using different concentrations of dry matter in the extract. (**B**) An average size of the ZnONPs prepared at different temperatures—estimates based on SEM micrographs. Values are the average of 15 measurements ± SD. Values with different letters indicate a significant difference, according to Tukey's test ($p < 0.05$).

3.2.5. DLS

Dynamic light scattering analysis determines the size and polydispersity index (PDI) based on the Brownian motions of the particles in the solution. It is an imperfect method that measures the hydrodynamic radius of the moving objects, and all the different sizes are measured together. Thus, the size distribution has a significant influence on the results. With a higher PDI, the results become more unreliable [71,72]. A PDI close to 0.1 corresponds to a monodisperse system, meaning that most of the particles in the media are the same size; in addition, this sample can be correctly analyzed using DLS. PDI values between 0.1–0.7 refer to a nearly monodisperse system. This might indicate that a higher proportion of the particles present in the media are monodisperse but that there is a distribution of particle sizes. In addition, PDI values higher than 0.7 correspond to a broad distribution of particle sizes present in the solution, and the DSL method cannot give reliable results. It can only be read as an estimation [72,73].

ZnONPs synthesized at a pH of 13, different extract concentrations, and different temperatures were analyzed using DLS to give average size, PDI, and zeta potential (ZP) (Figure 12). The average size, determined through DLS, of ZnONPs synthesized at given conditions depends strongly on the reaction temperature (Figure 12A). ZnONPs synthesized at lower temperatures have smaller average sizes (60–95 nm at 55 °C and 28–55 nm at 70 °C). Surprisingly, the synthesis at the lowest temperature yielded a rather large average size. The reason for that can be found in the long reaction time (15 h), proving that the extended-time reaction is unfavorable and leads to large sizes and aggregation. Confirming the SEM-images analysis, the synthesis at 85 °C resulted in the largest particles in the 102–145 nm range. DLS average sizes are larger than those determined from SEM images, which is most likely because nanoparticles observed in SEM were only seen on the surface of the agglomerates. In contrast, DLS measures the particles' three-dimensional radii, which might include a biomolecular coating. Such discrepancy between SEM and DLS average size has been reported before and is related to the specifics of the method used [74].

For all of the ZnONPs, the PDI values for most of the nanoparticles were around 0.2, representing nearly monodisperse systems (Figure 12B). Yet, the synthesis at the highest temperature and lowest extract concentration had a PDI of 0.39, suggesting that at that concentration, there is a low amount of the compounds to support well-defined particles.

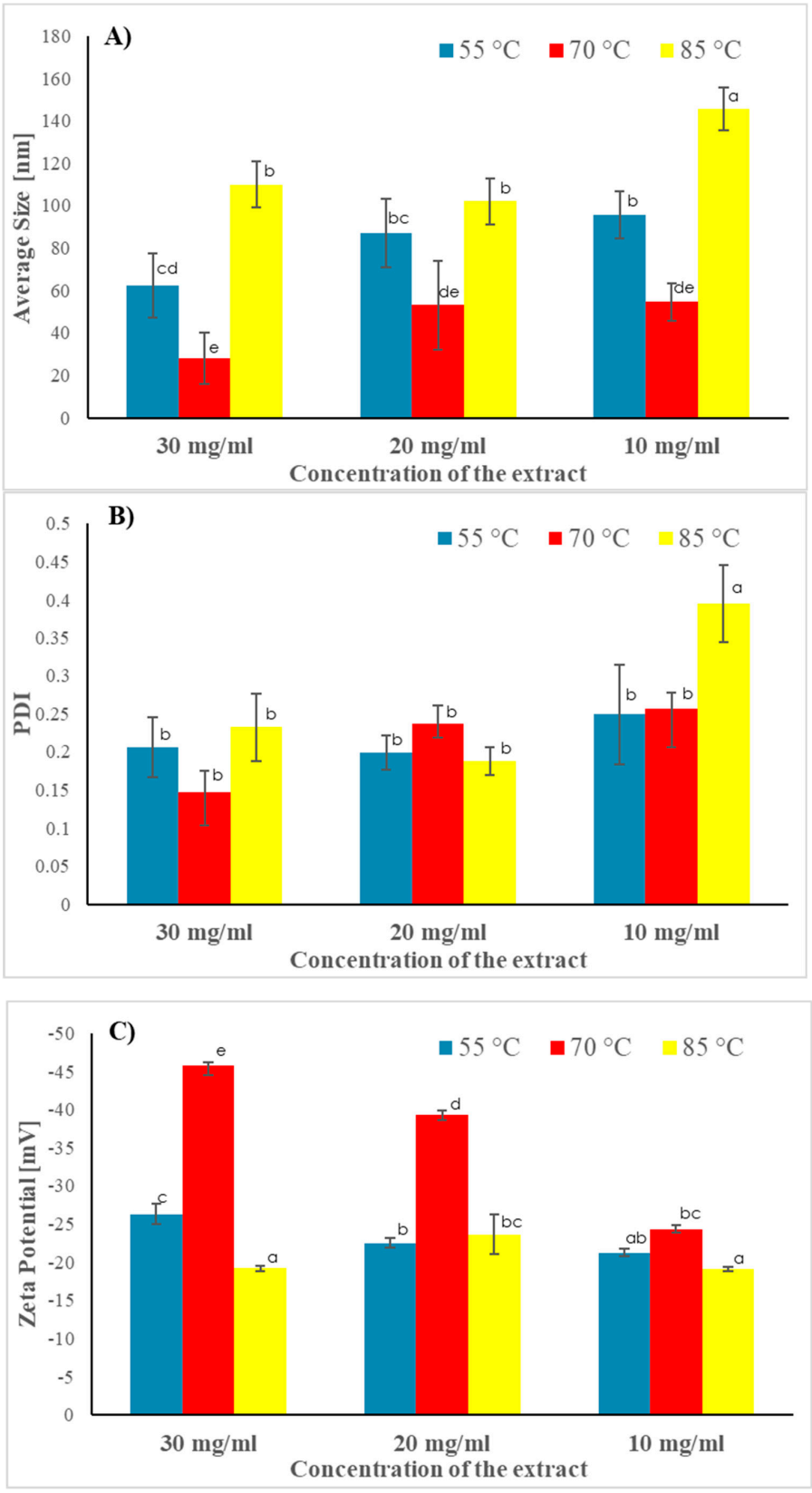

Figure 12. Average nanoparticles size (**A**), polydispersity index (PDI) (**B**), and zeta potential (**C**) determined by dynamic light scattering. The syntheses were run at pH of 13, different extract concentrations, and at different times depending on the temperature: 15 h at 55 °C, 4 h at 70 °C, and 2 h at 85 °C. Values are the average of three measurements. Values with different letters in the same column indicate a significant difference according to Tukey's test ($p < 0.05$).

The other factor determined from DLS is zeta potential, also termed electrokinetic potential, which is the potential at the shear plane of a colloid particle moving under an electric field. Dispersion stability can be suggested based on the value of ZP. Guidelines classify NP dispersions with ZP values of ±0–10 mV, ±10–20 mV, ±20–30 mV, and >±30 mV, as highly unstable, relatively stable, moderately stable, and highly stable, respectively [75]. All ZnONPs prepared here have a ZP below −20 mV (Figure 12C), which can be described as stable nanoparticle suspensions. However, the influence of extract concentration on the stability of the nanoparticles can be seen. ZnONPs prepared at 70 °C are the most stable when reduced by 30 and 20 mg/mL extract concentrations (ZP of −45.77 ± 0.36 and −39.26 ± 0.58 for 30 and 20 mg/mL, respectfully), which implies that the concentration of biocompounds is not only sufficient for efficient reduction (Figure 4) but also for forming a protective coating which supports dispersion [31].

The DLS results of average size, PDI, and ZP confirm that the best conditions for forming small, monodispersed, and well-stabilized ZnONPs are a pH of 13, a temperature of 70 °C, and an extract concentration of 30 mg/mL. The nanoparticles synthesized with these conditions have a size of 28.19 ± 5.2 nm, PDI of 0.147 ± 0.028, and zeta potential of −45.77 ± 0.36 mV.

3.3. Seed Germination

In general, the seed exposure to the ZnONPs resulted in the fresh weight of plumule and roots increasing compared to the control. Seeds exposed to 100 ppm ZnONPs had the highest masses of plume and roots and the longest roots, representing an increase by 19, 19, and 48%, respectively (Table 2). This increase may be related to the fact that zinc participates in the biosynthesis of endogenous hormones such as auxins and gibberellins [76], which are responsible for the cellular division that generates the elongation of the roots. In addition, zinc interferes with the metabolism of carbohydrates and proteins, resulting in escalated plumes' growth [77]. Similar findings were reported by Rai et al. [78], who noted higher growth in wheat seedlings after ZnONPs application on seeds.

Table 2. The measured parameters of seedling growth after 7 days of exposure to ZnONPs solutions.

Treatment ZnONP Concentration (ppm)	Plumule Fresh Weight (mg)	Root Fresh Weight (mg)	Length of the Roots (mm)
0	$11.24 \pm 0.02_{b}$	$1.80 \pm 0.08_{b}$	$12.27 \pm 0.40_{d}$
50	$10.10 \pm 0.21_{c}$	$1.61 \pm 0.04_{c}$	$15.03 \pm 0.52_{b}$
100	$13.41 \pm 0.21_{a}$	$2.15 \pm 0.09_{a}$	$18.21 \pm 0.21_{a}$
150	$11.77 \pm 0.52_{b}$	$1.88 \pm 0.20_{b}$	$14.37 \pm 0.05_{bc}$
200	$11.33 \pm 0.24_{b}$	$1.81 \pm 0.14_{b}$	$13.30 \pm 0.43_{dc}$
250	$12.20 \pm 0.08_{b}$	$1.95 \pm 0.07_{b}$	$9.31 \pm 0.25_{e}$

Values with different letters (a, b, c, d, e) within the same column indicate significant difference according to Tukey's test ($p \leq 0.05$). The values are the average of three repetitions. Means (n = 18) ± standard deviation.

Similarly, a higher percentage of germination was observed in seeds under most treatments with respect to the control (Figure 13A). The highest germination percentage was observed at 200 and 250 ppm of ZnONPs, representing an increase of 34 and 27%, respectively, with respect to the control. Such an effect could be attributed to the absorption of zinc oxide NPs which influences biochemical processes, such as hydrolysis or metabolism of inhibitors, imbibition, or activation of enzymes [78]. The results are consistent with those previously reported by Afrayeem et al. [79], who reported an increase in the germination percentage of *Capsicum annuum* L. seeds using 75 ppm ZnONPs [79]. The vigor index demonstrates a growth increase of 48% (Figure 13B), with respect to the control, for seeds treated with 200 ppm ZnONPs solution. Enhancing physiological parameters could be attributed to the quenching of free radicals by zinc oxide nanoparticles that entered the seeds through cracks in the seed coating. The 250 ppm treatment showed a decrease in the vigor index by 7% with respect to the control. The 250 ppm concentration represents the first ZnONP level to display phytotoxicity [80]. It has been proven that phytotoxicity

presents itself in germination as inhibition of root elongation [81], reductions in chlorophyll content [82], and decreased length of shoots [83]. The observed decrease in vigor index can be linked to the high osmotic potential of zinc, which often causes an inhibitory effect on seedlings' growth [14].

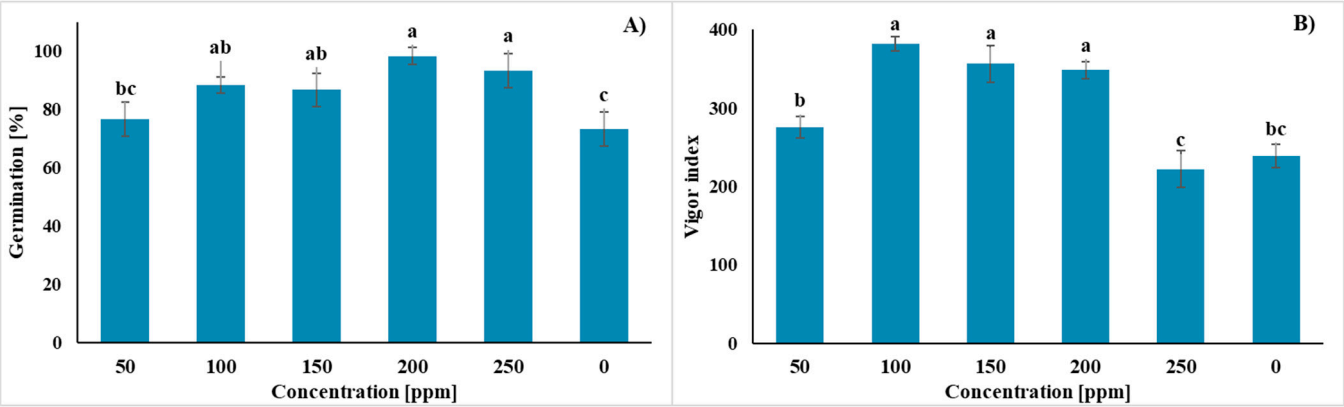

Figure 13. Percentage of the seed germination (**A**) and vigor index (**B**) with the treatment of ZnONPs at different concentrations (0 ppm indicated control without treatment). Values are the average of three measurements ± SD. Values with different letters indicate a significant difference, according to Tukey's test. ($p < 0.05$).

4. Conclusions

The ethanolic extracts of *Larrea tridentata* are capable of reducing zinc nitrate to zinc oxide nanoparticles, which replaces the use of toxic compounds in the synthesis of nanoparticles. UV-visible and FTIR spectroscopies, XRD, and SEM analyses confirmed the formation of pure, spherical, and uniform zinc oxide nanoparticles. The concentration of the extract is essential for the performance of the reaction. The higher the concentration, the faster the reaction and the higher the conversion of the ions into metallic particles without affecting the NPs' size or shape. In the same way, temperature is a factor of relevant importance in the synthesis of ZnONPs. Although low temperatures result in a slow reaction, the nanoparticles are spherical and with a small, uniform size. Increasing temperature speeds up the ZnONPs' formation but, at the same time, increases the possibility of aggregation and consolidation of the aggregates. Under acidic conditions, the formation of ZnONPs is incomplete, making separating the nanoparticles challenging. The synthesis at neutral pH also proceeds slowly, whereas a pH of 13 facilitates the reduction, resulting in well-defined and easily removable ZnONPs. Thus, the present study demonstrated that the best conditions for spherical and homogeneous ZnONPs are alkaline pH, 70 °C, and time under 4 h. Biosynthesized ZnONPs reduced by *Larrea tridentata* extracts stimulate serrano chili seeds' germination, and the seedling's growth.

Author Contributions: D.M.S.-P.: student on the project, investigation, data analysis, and writing of the original draft and review; E.F.-L.: conceptualization and writing: review and editing; S.Y.M.-G.: methodology and writing: review and editing; M.G.-G.: conceptualization and methodology; J.E.M.: conceptualization, investigation, methodology, project administration and writing: entire process. All authors have read and agreed to the published version of the manuscript.

Funding: This research received no external funding.

Institutional Review Board Statement: Not applicable.

Informed Consent Statement: Not applicable.

Data Availability Statement: The data presented in this study are available on request from the corresponding author.

Conflicts of Interest: The authors declare no conflict of interest.

References

1. Fouda, A.; Hassan, S.E.-D.; Salem, S.S.; Shaheen, T.I. In-Vitro cytotoxicity, antibacterial, and UV protection properties of the biosynthesized Zinc oxide nanoparticles for medical textile applications. *Microb. Pathog.* **2018**, *125*, 252–261. [CrossRef] [PubMed]
2. Lu, P.J.; Huang, S.C.; Chen, Y.P.; Chiueh, L.C.; Shih, D.Y.C. Analysis of titanium dioxide and zinc oxide nanoparticles in cosmetics. *J. Food Drug Anal.* **2015**, *23*, 587–594. [CrossRef]
3. Rastogi, A.; Tripathi, D.K.; Yadav, S.; Chauhan, D.K. Application of silicon nanoparticles in agriculture. *3 Biotech* **2019**, *9*, 90. [CrossRef] [PubMed]
4. González-Fernández, J.V.; Pinzón-Moreno, D.D.; Neciosup-Puican, A.A.; Carranza-Oropeza, M.V. Green Method, Optical and Structural Characterization of ZnO Nanoparticles Synthesized Using Leaves Extract of *M. oleifera*. *J. Renew. Mater.* **2022**, *10*, 833–847. [CrossRef]
5. Faizan, M.; Hayat, S.; Pichtel, J. Effects of Zinc Oxide Nanoparticles on Crop Plants: A Perspective Analysis. In *Sustainable Agriculture Review*; Springer: Berlin/Heidelberg, Germany, 2020; pp. 83–99. [CrossRef]
6. Rawal, T.B.; Ozcan, A.; Liu, S.-H.; Pingali, S.V.; Akbilgic, O.; Tetard, L.; O'Neil, H.; Santra, S.; Petridis, L. Interaction of Zinc Oxide Nanoparticles with Water: Implications for Catalytic Activity. *ACS Appl. Nano Mater.* **2019**, *2*, 4257–4266. [CrossRef]
7. Shkir, M.; Chandekar, K.V.; Alshehri, B.M.; Khan, A.; AlFaify, S.; Hamdy, M.S. A remarkable enhancement in photocatalytic activity of facilely synthesized Terbium@Zinc oxide nanoparticles. *Appl. Nanosci.* **2020**, *10*, 1811–1823. [CrossRef]
8. Kumar Sur, U.; Ankamwar, B.; Karmakar, S.; Halder, A.; Das, P. Green synthesis of Silver nanoparticles using the plant extract of Shikakai and Reetha. *Mater. Today Proc.* **2018**, *5*, 2321–2329. [CrossRef]
9. Swain, P.; Das, R.; Das, A.; Padhi, S.K.; Das, K.C.; Mishra, S.S. Effects of dietary zinc oxide and selenium nanoparticles on growth performance, immune responses and enzyme activity in rohu, *Labeo rohita* (Hamilton). *Aquac. Nutr.* **2019**, *25*, 486–494. [CrossRef]
10. Singh, J.; Kumar, S.; Alok, A.; Upadhyay, S.K.; Rawat, M.; Tsang, D.C.W.; Bolan, N.; Kim, K.-H. The potential of green synthesized zinc oxide nanoparticles as nutrient source for plant growth. *J. Clean. Prod.* **2019**, *214*, 1061–1070. [CrossRef]
11. Tymoszuk, A.; Wojnarowicz, J. Zinc oxide and zinc oxide nanoparticles impact on in vitro germination and seedling growth in *Allium cepa* L. *Materials* **2020**, *13*, 2784. [CrossRef]
12. Syu, Y.Y.; Hung, J.H.; Chen, J.C.; Chuang, H.W. Impacts of size and shape of silver nanoparticles on *Arabidopsis* plant growth and gene expression. *Plant Physiol. Biochem.* **2014**, *83*, 57–64. [CrossRef] [PubMed]
13. Kataria, S.; Jain, M.; Rastogi, A.; Živčak, M.; Brestic, M.; Liu, S.; Tripathi, D.K. Role of nanoparticles on photosynthesis: Avenues and applications. In *Nanomaterials in Plants, Algae and Microorganisms Concepts and Controversies: Volume 2*; Academic Press: Cambridge, MA, USA, 2018; Volume 2, pp. 103–127. [CrossRef]
14. Rajeshwari, A.; Kavitha, S.; Alex, S.A.; Kumar, D.; Mukherjee, A.; Chandrasekaran, N.; Mukherjee, A. Cytotoxicity of aluminum oxide nanoparticles on *Allium cepa* root tip—Effects of oxidative stress generation and biouptake. *Environ. Sci. Pollut. Res.* **2015**, *22*, 11057–11066. [CrossRef] [PubMed]
15. Sharma, A.; Patni, B.; Shankhdhar, D.; Shankhdhar, S.C. Zinc—An Indispensable Micronutrient. *Physiol. Mol. Biol. Plants* **2013**, *19*, 11–20. [CrossRef] [PubMed]
16. Yuvaraj, M.; Subramanian, K.S. Significance of Zinc Deficiency in Soil Zinc Interaction with Other Zinc Efficiency. *Biot. Res. Today* **2020**, *2*, 823–825.
17. Hassan, M.U.; Aamer, M.; Chattha, M.U.; Haiying, T.; Shahzad, B.; Barbanti, L.; Nawaz, M.; Rasheed, A.; Afzal, A.; Liu, Y.; et al. The critical role of zinc in plants facing the drought stress. *Agriculture* **2020**, *10*, 396. [CrossRef]
18. Bandeira, M.; Giovanela, M.; Roesch-Ely, M.; Devine, D.M.; da Silva Crespo, J. Green synthesis of zinc oxide nanoparticles: A review of the synthesis methodology and mechanism of formation. *Sustain. Chem. Pharm.* **2020**, *15*, 100223. [CrossRef]
19. Naveed Ul Haq, A.; Nadhman, A.; Ullah, I.; Mustafa, G.; Yasinzai, M.; Khan, I. Synthesis Approaches of Zinc Oxide Nanoparticles: The Dilemma of Ecotoxicity. *J. Nanomater.* **2017**, *2017*, 8510342. [CrossRef]
20. Reverberi, A.P.; Kuznetsov, N.T.; Meshalkin, V.P.; Salerno, M.; Fabiano, B. Systematical analysis of chemical methods in metal nanoparticles synthesis. *Theor. Found. Chem. Eng.* **2016**, *50*, 59–66. [CrossRef]
21. Jamkhande, P.G.; Ghule, N.W.; Bamer, A.H.; Kalaskar, M.G. Metal nanoparticles synthesis: An overview on methods of preparation, advantages and disadvantages, and applications. *J. Drug Deliv. Sci. Technol.* **2019**, *53*, 101174. [CrossRef]
22. Jadoun, S.; Arif, R.; Jangid, N.K.; Meena, R.K. Green synthesis of nanoparticles using plant extracts: A review. *Environ. Chem. Lett.* **2021**, *19*, 355–374. [CrossRef]
23. Nadaroğlu, H.; Alayli Güngör, A.; İnce, S. Synthesis of Nanoparticles by Green Synthesis Method. *Int. J. Innov. Res. Rev.* **2017**, *1*, 6–9.
24. Salayová, A.; Bedlovičová, Z.; Daneu, N.; Baláž, M.; Lukáčová Bujňáková, Z.; Balážova, Ľ.; Tkáčiková, Ľ. Green synthesis of silver nanoparticles with antibacterial activity using various medicinal plant extracts: Morphology and antibacterial efficacy. *Nanomaterials* **2021**, *11*, 1005. [CrossRef] [PubMed]
25. Córdova-Cisneros, K.C.; Sáenz-Galindo, A.; Ascacio-Valdés, J.A.; Narro-Cespedes, R.I.; Castañeda-Facio, A. Green synthesis of silver nanoparticles using the aqueous extract of *Larrea tridentate* and *Eucalyptus*. *Rev. Mex. Ing. Química* **2021**, *12*, 505–511. [CrossRef]

26. Lefebvre, T.; Destandau, E.; Lesellier, E. Selective extraction of bioactive compounds from plants using recent extraction techniques: A review. *J. Chromatogr. A* **2021**, *1635*, 461770. [CrossRef] [PubMed]
27. Farooq, A.; Khan, U.A.; Ali, H.; Satnish, M.; Naqvi, S.A.H.; Iqbal, S.; Ali, H.; Mubeen, I.; Amir, M.B.; Mosa, W.F.A.; et al. Green Chemistry Based Synthesis of Zinc Oxide Nanoparticles Using Plant Derivatives of *Calotropis gigantea* (Giant Milkweed). *Microorganisms* **2022**, *10*, 2195. [CrossRef] [PubMed]
28. Ahmed, S.S.; Alqahtani, A.M.; Alqahtani, T.; Alamri, A.H.; Menaa, F.; Mani, R.K.; Bharathi, D.R.; Kavitha, K. Green Synthesis, Characterizations of Zinc Oxide Nanoparticles from Aqueous Leaf Extract of *Tridax procumbens* Linn. *Materials* **2022**, *15*, 8202. [CrossRef]
29. Siddiqi, K.S.; ur Rahman, A.; Husen, T.; Husen, A. Properties of Zinc Oxide Nanoparticles and Their Activity Against Microbes. *Nanoscale Res. Lett.* **2018**, *13*, 482. [CrossRef]
30. Agarwal, H.; Kumar, S.V.; Rajeshkumar, S. A review on green synthesis of zinc oxide nanoparticles—An eco-friendly approach. *Resour. Effic. Technol.* **2017**, *3*, 406–413. [CrossRef]
31. Alhujaily, M.; Albukhaty, S.; Yusuf, M.; Mohammed, M.K.A.; Sulaiman, G.M.; Al-Karagoly, H.; Alyamani, A.A.; Albaqami, J.; AlMaiki, F. Recent Advances in Plant-Mediated Zinc Oxide Nanoparticles with Their Significant Biomedical Properties. *Bioengineering* **2022**, *9*, 541. [CrossRef]
32. Aguirre-Joya, J.A.; Pastrana-Castro, L.; Nieto-Oropeza, D.; Ventura-Sobrevilla, J.; Rojas-Molina, R.; Aguilar, C.N. The physico-chemical, antifungal and antioxidant properties of a mixed polyphenol based bioactive film. *Heliyon* **2018**, *4*, e00942. [CrossRef]
33. Bañuelos-Valenzuela, R.; Delgadillo-Ruiz, L.; Echavarría-Cháirez, F.; Delgadillo-Ruiz, O.; Meza-López, C. Composición química y ftir de extractos etanólicos de *Larrea tridentata*, *Origanum vulgare*, *Artemisa ludoviciana* y *Ruta graveolens*. *Agrociencia* **2018**, *52*, 309–321.
34. Manda, G.; Rojo, A.I.; Martínez-Klimova, E.; Pedraza-Chaverri, J.; Cuadrado, A. Nordihydroguaiaretic Acid: From Herbal Medicine to Clinical Development for Cancer and Chronic Diseases. *Front. Pharmacol.* **2020**, *11*, 572870. [CrossRef] [PubMed]
35. Floriano-Sánchez, E.; Villanueva, C.; Medina-Campos, O.N.; Rocha, D.; Sánchez-González, D.; Pedraza-Chaverrí, J.; Cárdenas-Rodríguez, N. Nordihydroguaiaretic acid is a potent in vitro scavenger of peroxynitrite, singlet oxygen, hydroxyl radical, superoxide anion and hypochlorous acid and prevents in vivo ozone-induced tyrosine nitration in lungs. *Free Radic. Res.* **2006**, *40*, 523–533. [CrossRef] [PubMed]
36. Singh, P.; Kim, Y.J.; Zhang, D.; Yang, D.C. Biological Synthesis of Nanoparticles from Plants and Microorganisms. *Trends Biotechnol.* **2016**, *34*, 588–599. [CrossRef] [PubMed]
37. Méndez-Andrade, R.; Vallejo-Perez, M.R.; Loera-Alvarado, E.; de los Santos-Villarreal, G.; García-Cerda, L.A.; Vera-Reyes, I. Efficacy of biosynthesized silver nanoparticles from *Larrea tridentata* against *Clavibacter michiganensis*. *J. Phytopathol.* **2022**, *170*, 91–99. [CrossRef]
38. Sánchez Ramírez, L.I. Nanopartículas Cu y CuO/Cu_2O Mediadas por Extracto de Larrea Tridentata y Su Potencial en la Remediación de Agua y Como Antimicrobiano. Master's Thesis, Cinvestav, Instituto Politécnico Nacional, Mexico City, Mexico, 2021.
39. Martins, S.; Aguilar, C.N.; De La Garza-Rodriguez, I.; Mussatto, S.I.; Teixeira, J.A. Kinetic study of nordihydroguaiaretic acid recovery from *Larrea tridentata* by microwave-assisted extraction. *J. Chem. Technol. Biotechnol.* **2010**, *85*, 1142–1147. [CrossRef]
40. Hasperué, J.H.; Rodoni, L.M.; Guardianelli, L.M.; Chaves, A.R.; Martínez, G.A. Use of LED light for Brussels sprouts postharvest conservation. *Sci. Hortic.* **2016**, *213*, 281–286. [CrossRef]
41. Brand-Williams, W.; Cuvelier, M.E.; Berset, C. Use of a free radical method to evaluate antioxidant activity. *LWT Food Sci. Technol.* **1995**, *28*, 25–30. [CrossRef]
42. Selim, Y.A.; Azb, M.A.; Ragab, I.; Abd El-Azim, M.H.M. Green Synthesis of Zinc Oxide Nanoparticles Using Aqueous Extract of *Deverra tortuosa* and their Cytotoxic Activities. *Sci. Rep.* **2020**, *10*, 3345. [CrossRef]
43. García-López, J.; Zavala-García, F.; Olivares-Sáenz, E.; Lira-Saldívar, R.H.; Barriga-Castro, E.D.; Ruiz-Torres, N.A.; Ramos-Cortez, E.; Vázquez-Alvarado, R.; Niño-Medina, G. Zinc Oxide nanoparticles boosts phenolic compounds and antioxidant activity of *Capsicum annuum* l. during germination. *Agronomy* **2018**, *8*, 215. [CrossRef]
44. Kujur, A.B.; Lal, G.M. Effect of hydropriming and osmopriming on germination behaviour and vigor of soybean (*Glycine max* L.) seeds. *Agric. Sci. Dig. Res. J.* **2015**, *35*, 207. [CrossRef]
45. Sarkhosh, S.; Kahrizi, D.; Darvishi, E.; Tourang, M.; Haghighi-Mood, S.; Vahedi, P.; Ercisli, S. Effect of Zinc Oxide Nanoparticles (ZnO-NPs) on Seed Germination Characteristics in Two Brassicaceae Family Species: *Camelina sativa* and *Brassica napus* L. *J. Nanomater.* **2022**, *2022*, 1892759. [CrossRef]
46. Yokosuka, A.; Iguchi, T.; Jitsuno, M.; Mimaki, Y. Structure and cytotoxicity of novel lignans and lignan glycosides from the aerial parts of *Larrea tridentata*. *Molecules* **2021**, *26*, 6186. [CrossRef] [PubMed]
47. Gnabre, J.; Bates, R.; Huang, R.C. Creosote bush lignans for human disease treatment and prevention: Perspectives on combination therapy. *J. Tradit. Complement. Med.* **2015**, *5*, 119–126. [CrossRef]
48. Ventura, J.; Belmares, R.; Aguilera-Carbo, A.; Gutiérrez-Sanchez, G.; Rodríguez-Herrera, R.; Aguilar, C.N. Fungal biodegradation of tannins from creosote bush (*Larrea tridentata*) and tar bush (*Fluorensia cernua*) for gallic and ellagic acid production. *Food Technol. Biotechnol.* **2008**, *46*, 213–217.
49. Choi, Y.S.; Jung, M.Y. Kinetic study on the singlet oxygen quenching activity of nordihydroguaiaretic acid (NDGA) using methylene blue sensitized photooxidation of α-terpinene. *Food Sci. Biotechnol.* **2016**, *25*, 1333–1336. [CrossRef]

50. Salmeron Martinez, W. Analisis Espectral en el Rango Ultravioleta Visible e Infrarrojo de los Exudados de *Eucalyptus globulus Labill*, *Corymbia citriodora Hook*, *Araucaria heterophylla*, *Mangifera indica* L., *Hymenaea courbaril* L. que se Encuentran dentro del Campus Central de la Universidad de El Salvador. Bachelor's Thesis, Universidad de El Salvador, San Salvador, El Salvador, 2017.
51. Douglas, P.; Burrows, H.D.; Evans, R.C. Foundations of Photochemistry. In *Applied Photochemistry*; Springer: Berlin/Heidelberg, Germany, 2013. [CrossRef]
52. Zhang, L.; Liu, Y.; Wang, Y.; Xu, M.; Hu, X. UV–Vis spectroscopy combined with chemometric study on the interactions of three dietary flavonoids with copper ions. *Food Chem.* **2018**, *263*, 208–215. [CrossRef]
53. Billinsky, J.L.; Marcoux, M.R.; Krol, E.S. Oxidation of the lignan nordihydroguaiaretic acid. *Chem. Res. Toxicol.* **2007**, *20*, 1352–1358. [CrossRef]
54. Manciu, F.S.; Guerrero, J.; Rivera, D.; Chang, S.Y.; Bennet, K.E. Combined theoretical and experimental study of nordihydroguaiaretic acid—From traditional medicine to modern spectroscopic research. *Biointerface Res. Appl. Chem.* **2020**, *10*, 6728–6743. [CrossRef]
55. Al Awadh, A.A.; Shet, A.R.; Patil, L.R.; Shaikh, I.A.; Alshahrani, M.M.; Nadaf, R.; Mahnashi, M.H.; Desai, S.V.; Muddapur, U.M.; Achappa, S.; et al. Sustainable Synthesis and Characterization of Zinc Oxide Nanoparticles Using Raphanus sativus Extract and Its Biomedical Applications. *Crystals* **2022**, *12*, 1142. [CrossRef]
56. Matinise, N.; Fuku, X.G.; Kaviyarasu, K.; Mayedwa, N.; Maaza, M. ZnO nanoparticles via *Moringa oleifera* green synthesis. *Appl. Surf. Sci.* **2017**, *406*, 339–347. [CrossRef]
57. Singh, A.K.; Pal, P.; Gupta, V.; Yadav, T.P.; Gupta, V.; Singh, S.P. Green synthesis, characterization and antimicrobial activity of zinc oxide quantum dots using *Eclipta alba*. *Mater. Chem. Phys.* **2018**, *203*, 40–48. [CrossRef]
58. Velgosová, O.; Mražiková, A.; Marcinčáková, R. Influence of pH on green synthesis of Ag nanoparticles. *Mater. Lett.* **2016**, *180*, 336–339. [CrossRef]
59. Ogunyemi, S.O.; Abdallah, Y.; Zhang, M.; Fouad, H.; Hong, X.; Ibrahim, E.; Masum, M.M.I.; Hossain, A.; Mo, J.; Li, B. Green synthesis of zinc oxide nanoparticles using different plant extracts and their antibacterial activity against *Xanthomonas oryzae* pv. oryzae. *Artif. Cells Nanomed. Biotechnol.* **2019**, *47*, 341–352. [CrossRef]
60. Ishwarya, R.; Vaseeharan, B.; Kalyani, S.; Banumanthi, B.; Govindarajan, M.; Alharbi, N.S.; Kadaikunnan, S.; Al-anbr, M.N.; Khaled, J.M.; Benelli, G. Facile green synthesis of zinc oxide nanoparticles using *Ulva lactuca* seaweed extract and evaluation of their photocatalytic, antibiofilm and insecticidal activity. *J. Photochem. Photobiol. B Biol.* **2018**, *178*, 249–258. [CrossRef]
61. Dobrucka, R.; Długaszewska, J. Biosynthesis and antibacterial activity of ZnO nanoparticles using *Trifolium pratense* flower extract. *Saudi J. Biol. Sci.* **2016**, *23*, 517–523. [CrossRef]
62. Eyaane Meva, F.; Segnou, M.L.; Ebongue, C.O.; Ntoumba, A.A.; Kedi, P.B.E.; Deli, V.; Etoh, M.-A.; Mpondo, E.M. Spectroscopic synthetic optimizations monitoring of silver nanoparticles formation from *Megaphrynium macrostachyum* leaf extract. *Rev. Bras. Farmacogn.* **2016**, *26*, 640–646. [CrossRef]
63. Irfan, M.; Munir, H.; Ismail, H. *Moringa oleifera* gum based silver and zinc oxide nanoparticles: Green synthesis, characterization and their antibacterial potential against MRSA. *Biomater. Res.* **2021**, *25*, 17. [CrossRef]
64. Shaziman, S.; Ismailrosdi, A.S.; Mamat, M.H.; Zoolfakar, A.S. Influence of Growth Time and Temperature on the Morphology of ZnO Nanorods via Hydrothermal. *IOP Conf. Ser. Mater. Sci. Eng.* **2015**, *99*, 012016. [CrossRef]
65. Zare, E.; Pourseyedi, S.; Khatami, M.; Darezereshki, E. Simple biosynthesis of zinc oxide nanoparticles using nature's source, and it's in vitro bio-activity. *J. Mol. Struct.* **2017**, *1146*, 96–103. [CrossRef]
66. Fakhari, S.; Jamzad, M.; Fard, H.K. Green synthesis of zinc oxide nanoparticles: A comparison. *Green Chem. Lett. Rev.* **2019**, *12*, 19–24. [CrossRef]
67. Vijayakumar, S.; Mahadevan, S.; Arulmozhi, P.; Sriram, S.; Praseetha, P.K. Green synthesis of zinc oxide nanoparticles using *Atalantia monophylla* leaf extracts: Characterization and antimicrobial analysis. *Mater. Sci. Semicond. Process.* **2018**, *82*, 39–45. [CrossRef]
68. Vimala, K.; Sundarraj, S.; Paulpandi, M.; Vengatesan, S.; Kannan, S. Green synthesized doxorubicin loaded zinc oxide nanoparticles regulates the Bax and Bcl-2 expression in breast and colon carcinoma. *Process Biochem.* **2014**, *49*, 160–172. [CrossRef]
69. Chikkanna, M.M.; Neelagund, S.E.; Rajashekarappa, K.K. Green synthesis of Zinc oxide nanoparticles (ZnO NPs) and their biological activity. *SN Appl. Sci.* **2019**, *1*, 117. [CrossRef]
70. Alwan, R.M.; Kadhim, Q.A.; Sahan, K.M.; Ali, R.A.; Mahdi, R.J.; Kassim, N.A.; Jassim, A.N. Synthesis of Zinc Oxide Nanoparticles via Sol–Gel Route and Their Characterization. *Nanosci. Natnothecnol.* **2015**, *5*, 1–6. [CrossRef]
71. Singh, P.; Kim, Y.J.; Singh, H.; Wang, C.; Hwang, K.H.; Farh, M.E.-A.; Yang, D.C. Biosynthesis, characterization, and antimicrobial applications of silver nanoparticles. *Int. J. Nanomed.* **2015**, *10*, 2567–2577. [CrossRef]
72. Stetefeld, J.; McKenna, S.A.; Patel, T.R. Dynamic light scattering: A practical guide and applications in biomedical sciences. *Biophys. Rev.* **2016**, *8*, 409–427. [CrossRef]
73. de Freitas Rosa, P.; Cirqueira, S.S.R.; Aguiar, M.L.; Bernardo, A. Synthesis and characterization of silver nanoparticles. *Mater. Sci. Forum* **2014**, *802*, 135–139. [CrossRef]
74. Jafarirad, S.; Mehrabi, M.; Divband, B.; Kosari-nasab, M. Biofabrication of zinc oxide nanoparticles using fruit extract of *Rosa canina* and their toxic potential against bacteria. *Mater. Sci. Eng. C* **2016**, *59*, 296–302. [CrossRef]
75. Bhattacharjee, S. DLS and zeta potential—What they are and what they are not? *J. Control. Release* **2016**, *235*, 337–351. [CrossRef]

76. Seleiman, M.F.; Almutairi, K.F.; Alotaibi, M.; Shami, A.; Alhammad, B.A.; Battaglia, M.L. Nano-fertilization as an emerging fertilization technique: Why can modern agriculture benefit from its use? *Plants* **2021**, *10*, 2. [CrossRef]
77. Suganya, A.; Saravanan, A.; Manivannan, N. Role of Zinc Nutrition for Increasing Zinc Availability, Uptake, Yield, and Quality of Maize (*Zea Mays* L.) Grains. *Commun. Soil Sci. Plant Anal.* **2020**, *51*, 2001–2021. [CrossRef]
78. Rai-Kalal, P.; Jajoo, A. Priming with zinc oxide nanoparticles improve germination and photosynthetic performance in wheat. *Plant Physiol. Biochem.* **2021**, *160*, 341–351. [CrossRef] [PubMed]
79. Afrayeem, S.M.; Chaurasia, A.K. Effect of zinc oxide nanoparticles on seed germination and seed vigour in chilli (*Capsicum annuum* L.). *J. Pharmacogn. Phytochem.* **2017**, *6*, 1564–1566.
80. Song, U.; Lee, S. Phytotoxicity and accumulation of zinc oxide nanoparticles on the aquatic plants *Hydrilla verticillata* and *Phragmites australis*: Leaf-type-dependent responses. *Environ. Sci. Pollut. Res.* **2016**, *23*, 8539–8545. [CrossRef] [PubMed]
81. Chen, J.; Dou, R.; Yang, Z.; You, T.; Gao, X.; Wang, L. Plant Physiology and Biochemistry Phytotoxicity and bioaccumulation of zinc oxide nanoparticles in rice (*Oryza sativa* L.). *Plant Physiol. Biochem.* **2018**, *130*, 604–612. [CrossRef] [PubMed]
82. Kaur, H.; Garg, N. Zinc toxicity in plants: A review. *Planta* **2021**, *253*, 129. [CrossRef]
83. Balážová, Ľ.; Babula, P.; Baláž, M.; Bačkorová, M.; Bujňáková, Z.; Briančin, J.; Kurmanbayeva, A.; Sagi, M. Zinc oxide nanoparticles phytotoxicity on halophyte from genus *Salicornia*. *Plant Physiol. Biochem.* **2018**, *130*, 30–42. [CrossRef] [PubMed]